Carbon Vol. 18, pp. 169–178

0008-6223/80/0601-0169/$02.00/0

SUBCRITICAL CRACK GROWTH IN FINE GRAINED POLYCRYSTALLINE GRAPHITES

J. L. WOOD,† R. C. BRADT and P. L. WALKER, JR.

Department of Materials Science and Engineering, The Pennsylvania State University, University Park, PA 16802, U.S.A.

(*Received* 26 *September* 1979)

Abstract—Subcritical crack growth was measured in four fine grained polycrystalline graphites in air at room temperature. Filler and textural effects were observed at stress intensity factors (K_I) near the critical stress intensity (K_{Ic}). Scanning electron microscope fractography permitted correlation with processing conditions and microstructure. The results are compared with those for other carbon materials.

1. INTRODUCTION

Graphites are being increasingly utilized for structural, load bearing applications. In some of these applications, subcritical crack growth in the graphite precedes mechanical failure. Consequently, determination of subcritical crack growth characteristics and associated mechanism(s) are of primary engineering and theoretical importance.

Diefendorf [1] appears to be the first investigator to observe the delayed failure of graphitic materials at room temperature, coincidentally for the Airco Speer grade 580 also tested in this study. He reported a 10% increase in the flexural strength of this material when tested in vacuum (10^{-11}MN/m^2) as compared to testing in air. Diefendorf theorized that adsorption of gases (present in the as-received graphite) on internal pore surfaces was responsible for a stress corrosion effect. Rowe [2] similarly observed that degassing at elevated temperatures increased both the elastic modulus and the strength when these properties were measured in vacuum at room temperature. Both of these properties returned to their as-received levels if the air was readmitted to the test chamber. Logsdail [3] and Vitovec and Stachurski [4], using bend tests at room temperature, concluded that the presence of water vapor in air leads to a reduction in the strength of polycrystalline graphites.

Several investigators have recently utilized fracture mechanics techniques to examine the slow crack growth of graphites at room temperature. Freiman and Mecholsky [5], applying the double-torsion technique, found only a single, environmentally-insensitive region of stress intensity-crack velocity behavior. In that region, they reported that the presence of adsorbed gases acted to enhance slow crack growth in two graphites (POCO AXF-5Q and Union Carbide ATJ-S). They also observed significant crack growth anisotropy in the molded ATJ-S material. In particular, they found that the most resistant orientation to slow crack growth was that in which the crack propagated perpendicular to the graphite lamellae, while the weakest was that in which the crack propagated between or parallel to the plane of the lamellae. Nadeau and Hodkinson [6], also using the double-torsion method, reported that slow crack growth in three graphites, POCO AXZ, AXF-5Q, and ESP Union Carbide pyrolytic graphite, occurs only at large fractions of K_{Ic}, and attributed it primarily to mechanical failure.

The micromechanics of fracture in graphites has also received some attention [7–11]. Primary crack extension has been modelled to occur by the linking of secondary cracks, frequently initiating at pores in advance of the main crack. Cracks propagate along the striations in the filler particles, or by a cleavage process in suitably oriented filler particles. Most studies report that crack initiation in advance of the main crack occurs at stress levels which are below the failure stress, an observation that receives some confirmation by acoustic emission studies [12–14].

It has been established that subcritical or slow crack growth occurs in graphite, having been observed through conventional strength tests as well as fracture mechanics techniques. It is the objective of the present study to examine the effects of fillers, selected processing conditions and microstructure on slow crack growth in several fine grain size polycrystalline graphites and to compare the results with other carbon materials.

2. EXPERIMENTAL PROCEDURE

2.1 *Preparation of artifacts*

Four commercial graphites‡ were examined in this study. Information on the fillers and forming methods are listed in Table 1. Artifacts based on petroleum coke were produced by mixing of the filler with coal

†Present address: Bendix Aircraft Brake & Strut Division, 3520 W. Westmoor St., P.O. Box 10, South Bend, IN 46624, U.S.A.

‡Airco Speer Carbon-Graphite, St. Marys, Pennsylvania, U.S.A.

Table 1. Fabrication information for the artifacts

Grade	Filler	Maximum Filler Size (μm)	Forming Process	Artifact Dimensions (in)
580	Petroleum Coke	200	Extrusion	3.5 x 48
3499	Petroleum Coke	75	Molding	12 x 12 x 2.5
KK-16	Petroleum Coke	20	Isostatic Molding	12 x 6 x 2
4029	Lampblack	125	Molding	10 x 4 x 2

tar pitch, forming, baking and subsequent graphitization. In contrast, a preforming process was applied to the production of the artifact based on lampblack. The lampblack filler was mixed with a binder, then formed and carbonized. The carbonized body was subsequently milled and sized, then mixed with additional pitch, formed, baked and graphitized to produce the final artifact.

2.2 *Characterization and mechanical property measurements*

Macropore size distributions were obtained by mercury porosimetry. Helium, X-ray and apparent densities were used to determine the open and closed porosity. The apparent densities were calculated from the specimen mass and dimensions.

Elastic properties (Young's modulus, E, and shear modulus, G) were determined by dynamic mechanical resonance techniques [15]. The shear modulus was determined from the torsional resonance while Young's modulus and Poisson's ratio (ν) were determined using the flexural resonance and an iteration process based on

$$\nu = (E/2G) - 1. \quad (1)$$

Although this equation is only applicable to isotropic solids, it is a satisfactory approximation for most polycrystalline ceramic materials. Apparent density and elastic property values represent the mean and 95% confidence limits for 25 samples.

To determine interlayer spacings, solid samples of each graphite (35 mm × 10 mm × 5 mm) were compared with a 200-mesh sodium chloride internal standard. The (002) and (004) peaks of graphite and the (111), (200), (220) and (222) peaks of sodium chloride were observed in the analysis. The experimental d-values of sodium chloride were compared with the absolute values calculated from its lattice constant of 2.800 Å at 25 ± 1°C. A plot of experimental error in angle of the (111) peak at $2\theta = 27.4°$, (200) peak at $2\theta = 31.7°$, (220) peak at $2\theta = 45.5°$ and the (222) at $2\theta = 56.5°$ was used to determine the error in the angle of the (002) and (004) peaks of graphite at approx. 26.5° and 54.5° respectively. The corrected 2θ angles were then used to compute the interlayer spacing using Bragg's Law. Crystallite alignment was obtained through X-ray analysis of the intensity ratio for the (002) diffraction peak in the transverse (T) orientation compared to that in the longitudinal (L) orientation (see Figs. 1 and 2).

The double-torsion test [16] was applied to measure slow crack growth in these graphites at 22°C and 40% relative humidity. Specimens (76 mm × 25 mm × 6 mm), also used for apparent density and elastic property measurements, were cut from artifacts in the longitudinal (L) orientation for the extruded grade and in the transverse (T) and longitudinal (L) orientations for the molded materials (Fig. 1). For the extruded grade, 580, the longitudinal sample has its long dimension parallel to the extrusion direction. In the molded grades, 3499 and 4029, the transverse sample has its plane of maximum area perpendicular to the molding direction. The longitudinal sample in the molded grades has its plane of intermediate area perpendicular to the molding direction. For the isostatically molded grade, KK-16, longitudinal and transverse specimens were cut in orientations corresponding to those for 3499 and 4029, as if KK-16 had

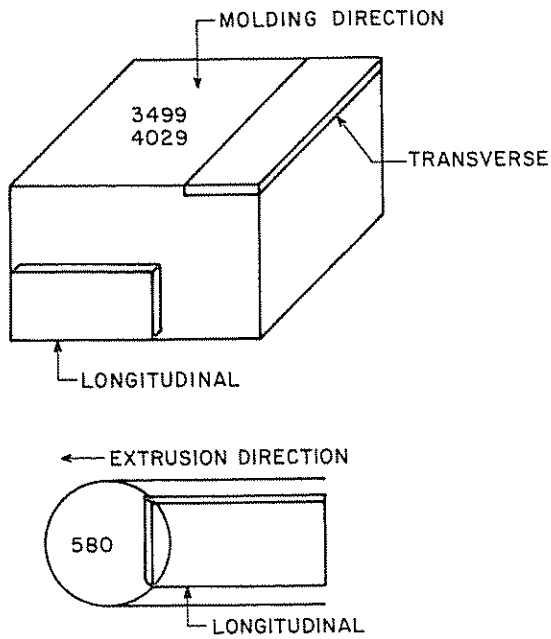

Fig. 1. Artifacts of the graphites with double-torsion specimen orientations indicated.

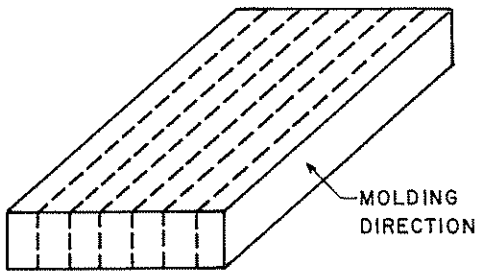

LONGITUDINAL

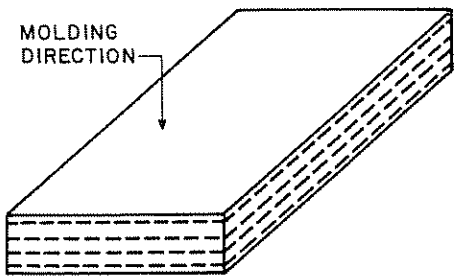

TRANSVERSE

Fig. 2. Longitudinal and transverse specimens showing preferential basal plane alignment (grades 3499 and 580) and molding directions (grades 3499 and 4029).

been unidirectionally molded in a direction perpendicular to the major surface of the artifact. The dashed lines are added to Fig. 2 to suggest that some preferential alignment of basal planes is expected (as a function of forming direction) for samples of 3499 and 580, where petroleum coke is the filler. It must be pointed out that, for the molded materials, "longitudinal" does not refer to a specimen with its long dimension parallel to the molding direction. To clearly illustrate microstructural effects on slow crack growth, "longitudinal" is used to refer to the molded specimen with crystallite alignment identical to that for longitudinal specimens of the extruded grade (Fig. 2).

In the double-torsion method (Fig. 3), a large, artificial crack is introduced into the specimen during loading. A groove (0.8 mm wide by 3 mm deep) aided crack propagation along the center-line of the specimen. Noting that the crack propagates along the center line of the double-torsion specimen, it is evident, from Fig. 2, that the fracture path in the longitudinal sample is parallel to the basal planes of the crystallites, the easy cleavage direction. Conversely, the transverse specimens fracture in a direction perpendicular to the basal planes of the crystallites, a tougher direction.

In the load relaxation test, a slow crosshead speed, typically 2×10^{-6} m/sec, is applied to the double-torsion specimen until the load levels off to a constant value, indicative of crack motion. The crosshead is instantaneously arrested and the load allowed to relax. The relaxation time is typically a few minutes, long enough to ultimately result in measurable slow crack velocities, between 10^{-2} and 10^{-6} m/sec. By unloading and reloading the specimen, multiple load relaxation curves can be obtained from a single sample. The crack velocity (V) and associated opening mode stress intensity (K_I) were calculated from the load relaxation using the following equations given elsewhere [17]:

$$V = [\dot{y}\, P_0/\dot{P}_0 B]\,(\dot{P}/P^2) \tag{2}$$

where $\dot{y}$ is the crosshead speed, P_0 is the initial (and maximum) load of load relaxation curve, $\dot{P}_0$ is the initial slope of load relaxation curve, P is the load at any point along load relaxation curve, $\dot{P}$ is the slope of load relaxation curve at P, B is the specimen compliance $= 3W_m^2/Wt^3G$

where W_m is the distance between upper and lower load points, W is the specimen width, t is the specimen thickness, G is the shear modulus and

$$K_I = PW_m\left[\frac{3(1+\nu)}{Wt^3t_n}\right]^{1/2} \tag{3}$$

where ν is the Poisson's ratio and t_n is the specimen web thickness.

K_{Ic}, the fracture toughness, is measured by the same configuration at a higher crosshead speed typically 4×10^{-5} m/sec.

The range of crack velocities easily measured by the load relaxation technique is limited to 10^{-2}–10^{-6} m/sec. The upper limit is governed by the length of the specimen and the lower limit is imposed by spurious relaxations of the testing device or by temperature variations. Load relaxation curves were digitized using a Numonics Electronic Graphics Calculator. Using computer techniques [18], the digitized data were subsequently converted to stress intensity factor (K_I)-crack velocity (V) values and plotted as a log V_I–log K_I relationship using a Tektronix 4662 Plotter.

Slow crack growth data are conveniently illustrated on a (K_I–V_I) diagram such as schematically depicted in Fig. 4. In the most general case, four regions of

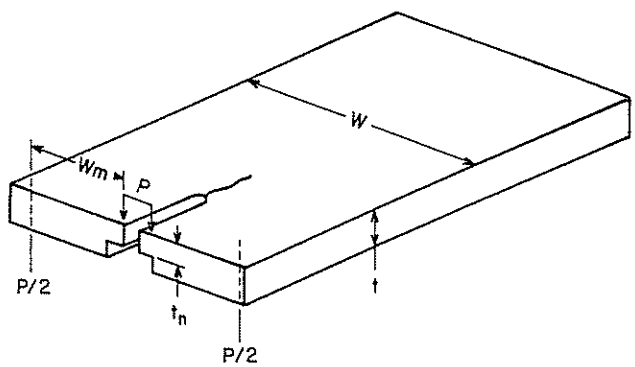

Fig. 3. Double-torsion loading configuration.

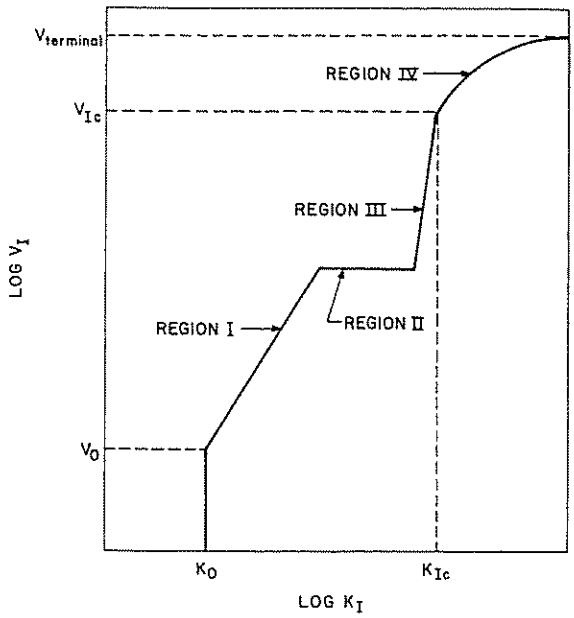

Fig. 4. Schematic (K_I-V_I) diagram.

behavior are observed. The point (K_0, V_0), the fatigue limit, represents the lower limit of stress corrosion behavior. Region I, describing velocities just larger than V_0, can be represented by a straight line on a log V_I–log K_I plot. It is described by the empirical equation:

$$V_I = AK_I^N \tag{4}$$

where V_I is the crack velocity, K_I is the mode I stress intensity factor, and A and N are constants. A crack-tip, stress-corrosion reaction is usually assumed to be rate-controlling in Region I.

In Region II, the crack velocity exceeds the speed of corrosive-species mass transport to the crack tip. In this region, diffusion of the corrosive species is the rate-controlling step for crack advancement. Crack velocity is not a function of the stress intensity factor. Crack extension in Region III is generally attributed to mechanical failure. Equation (4) also appropriately describes Region III. The crack approaches the critical velocity, V_{Ic}, as the stress intensity approaches K_{Ic}. In Region IV, the crack velocity accelerates from V_{Ic} ($\sim 10^{-1}$ m/sec) to the terminal velocity, represented by the speed of sound in the material and determined by the material's elastic constants.

Both Regions I and III are characterized by the stress intensity exponent, N, a measure of the material's resistance to the slow crack growth process. For materials which exhibit both regions of slow crack growth behavior under similar experimental conditions, the Region III N-value is consistently larger than that in Region I, indicating that crack velocity is more sensitive to incremental changes in K_I in Region III.

Fracture surfaces of all specimens were examined by scanning electron microscopy (SEM) methods.

3. RESULTS AND DISCUSSION

3.1 *Materials characterization*

The four graphites studied are fine grained, highly porous materials, as seen in Table 2. These materials consist of large amounts of open porosity and a significant percentage of closed porosity. Mean macropore sizes were determined by locating maxima on a differential mercury penetration plot (Fig. 5). A second, less pronounced maximum, located at 0.3 μm in grade 4029, is indicative of porosity within the lampblack-binder particles produced during the preforming processing steps previously detailed.

Interlayer spacings indicate that the petroleum coke-filled grades are well-graphitized, approaching the theoretical value of 3.354 Å. The lampblack-filled grade is the least graphitized of the four. X-ray analysis of crystallite alignment is in agreement with intuitive reasoning, based upon the processing of each grade. The molded petroleum coke-filled graphite, 3499, is most anisotropic grade with regard to X-rays, with $I_T/I_L = 2.09$. The extruded grade, 580, is anisotropic, while the lampblack-filled grade, 4029, is nearly isotropic. Isostatically pressed KK-16 is also

Table 2. Selected properties of the graphites

Grade	Apparent Density gm/cc	Porosity (%) Open	Closed	Total	Mean Macropore Size (μm)	Interlayer Spacing d_{002} (Å)	X-Ray Crystallite Alignment (I_T/I_L)		E MN/m^2 ($\times 10^{-3}$)	G MN/m^2 ($\times 10^{-3}$)	ν
580	1.70±.004	22.8	1.9	24.7	2–5	3.364	1.62	L	13.57 ±.21	6.27 ±.14	0.09 ±.02
3499	1.71±.003	17.8	6.4	24.2	5	3.368	2.09	L	9.65 ±.07	3.58 ±.02	0.38 ±.01
								T	9.44 ±.07	3.63 ±.005	0.09 ±.007
KK-16	1.84±.002	12.5	5.9	18.4	1.5	3.370	0.89	L	12.40 ±.07	4.34 ±.03	0.11 ±.003
								T	12.54 ±.07	5.65 ±.03	0.11 ±.004
4029	1.46±.002	29.0	5.3	34.3	4–5	3.408	1.05	L	5.31 ±.06	2.20 ±.03	0.19 ±.009
								T	5.03 ±.14	2.07 ±.04	0.20 ±.006

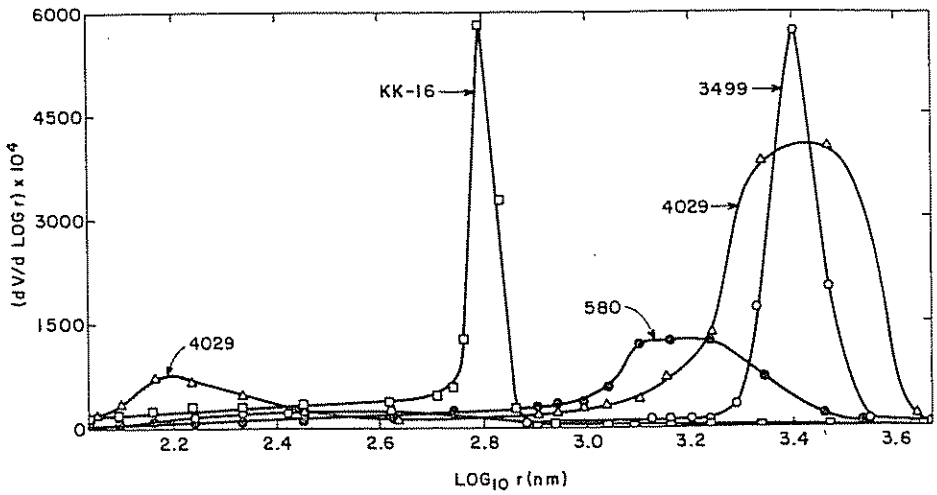

Fig. 5. Differential mercury penetration into artifacts

nearly isotropic. Due to relatively high amounts of binder in grade 4029, however, the structure of the filler phase may not be wholly resolved by the X-ray analysis.

Elastic moduli of the petroleum coke-filled grades are higher than those for the lampblack-filled grade. The lower moduli of grade 4029 are consistent with its lower apparent density. For the three grades on which directional measurements were made, the transverse (T) and longitudinal (L) moduli are approximately equal. This is to be expected for grade 3499 since the moduli are measured in directions perpendicular to the forming direction, that is in the plane of orthotropic symmetry of this graphite. It is also expected for grades KK-16 and 4029, which show negligible preferred crystallite alignment as measured by X-ray diffraction.

3.2 *Subcritical crack growth*

Slow crack growth in these polycrystalline graphites is conveniently represented on the standard (K_I–V_I) diagram. Figure 6 illustrates such a diagram of experimental results for the extruded grade 580. It includes data representing four separate relaxations for each of two different specimens. Treating all eight of the relaxations in a single regression analysis of eq. (4), $V_I = AK_I^N$, yields a correlation coefficient, $R^2 = 0.97$, clearly indicating the applicability of the empirical equation, as well as the reproducibility of the data. Values of N and $\log A$ for this particular material are 215 ± 14 and -1304 ± 84 respectively.

Figure 6 illustrates that only a single region of stress intensity-crack velocity behavior is observed. Previously, when only a single region has been observed, it has been designated as either mechanically-controlled Region III behavior [6], or as Region I behavior [5] in which stress corrsoion enhances slow crack growth. The $(K_I)_{min}$ value, the minimum stress intensity measured during a relaxation, indicates that the slow crack growth detected in grade 580 occurs only at $K_I > 0.96\,K_{Ic}$, in agreement with the observation of Nadeau [6] that high fractions of K_{Ic} are necessary for slow crack growth in graphite. Extrapolation of the data in Fig. 6 to K_{Ic} results in a reasonable value of V_{Ic}, about 10^{-1}–10^{-2} m/sec, implying that a transition into another region of slow crack growth behavior prior to reaching K_{Ic} is highly unlikely. The slow crack growth measured in grade 580 must be Region III. This interpretation is further substantiated by analogy with three other brittle materials for which distinct Region I and Region III slow crack growths have been observed; a soda lime silicate glass, single crystal sapphire, and a polycrystalline alumina. Analysis of the data reviewed by Wiederhorn [19] reveals that Region I behavior is observed for the respective three

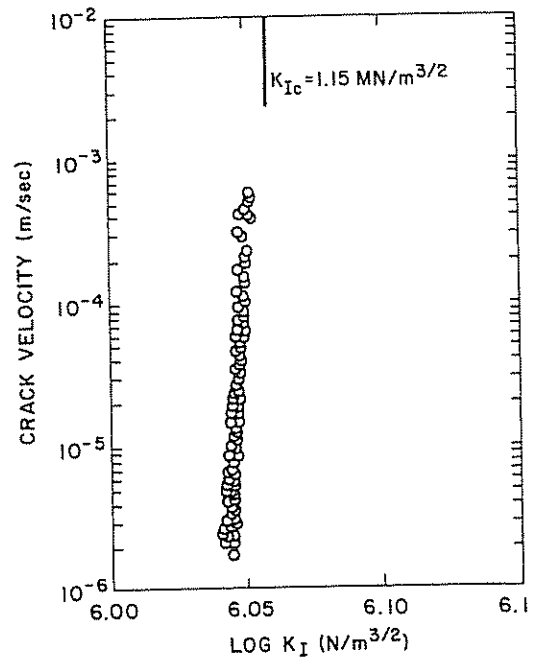

Fig. 6. Slow crack growth in grade 580.

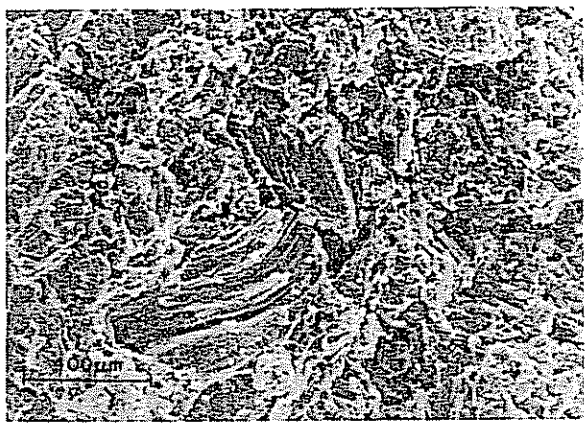

Fig. 7. Longitudinal fracture surface of grade 580.

materials at (0.63–0.78), (0.11–0.57), and (0.59–0.74) of their respective K_{Ic} values. Region III behavior is observed only at very large fractions, (>0.89), (>0.83) and (>0.93) of their respective K_{Ic} values. These results, coupled with the high N value, and with the large $(K_{I_{min}}/K_{Ic})$ ratio, indicate that the slow crack growth measured in grade 580 at room temperature is Region III crack growth, primarily determined by mechanical failure, rather than Region I determined by a stress corrosion mechanism.

The micromechanics of slow crack growth in grade 580 are clearly revealed by the SEM fractography. Fracture in this material occurs by a combination of binder phase failure and cleavage of the large filler particles (Fig. 7). However, cleavage only appears to occur in those filler particles whose basal planes are nearly perpendicular to the applied stress. Numerous fractured filler particles are observed, in agreement with the preferred crystallite alignment in the longitudinal orientation of this grade, as indicated by X-ray analysis.

The other three grades measured in this study also exhibit only a single region of slow crack growth behavior. This region, characterized by high N values (Table 3), is similarly observed only at large fractions of these materials' respective K_{Ic}'s (Table 4). In addition, significant crack growth anisotropy is observed

Table 3. Room temperature slow crack growth parameters

Grade	Orientation	Slope ($m^{5/2}/N \cdot sec$)	Intercept Log A
580	L	215±14	-1304±34
3499	L	198±10	-1192±61
	T	149±13	- 909±80
KK-16	L	152±27	- 933±164
	T	298±22	-1836±133
4029	L	224±29	-1270±165
	T	185±12	-1067±67

Table 4. Stress intensity values for the graphites

Grade	Orientation	K_{Ic} ($MN/m^{3/2}$)	$\left(\frac{K_{I_{MIN}}}{K_{Ic}}\right)$
580	L	1.15	0.96
3499	L	1.00	0.96
	T	1.20	0.95
KK-16	L	1.36	0.94
	T	1.43	0.97
4029	L	0.457	0.95
	T	0.596	0.95

for grades 3499 and 4029. For isostatically molded grade KK-16, crack growth is nearly isotropic with regard to the toughness and stress intensities observed during crack propagation.

In agreement with the preferred alignment of basal planes in grade 3499, considerable slow crack growth anisotropy also is observed (Fig. 8). As expected from the crystallite orientation schematically depicted in Fig. 2, the transverse orientation is tougher than the longitudinal orientation. Fractography reveals that crack front-microstructural interactions are responsible for this anisotropy, as extensive cleavage of the large petroleum coke particles is apparent in the longitudinal orientation (Fig. 9a). In contrast, the transverse fracture surfaces reveal extremely tortuous crack paths, including regions in which filler particle fractures appear to be perpendicular to the layer planes (Fig. 9b).

As expected, slow crack growth in the isostatically molded grade, KK-16, is nearly isotropic, with a

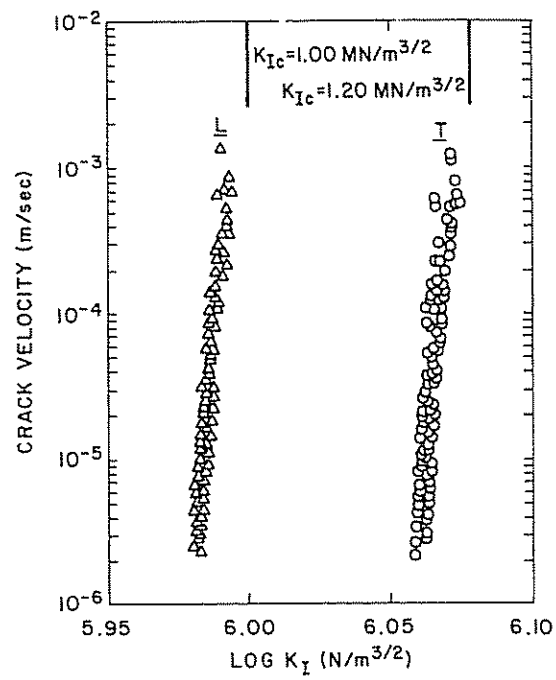

Fig. 8. Anisotropic slow crack growth in grade 3499.

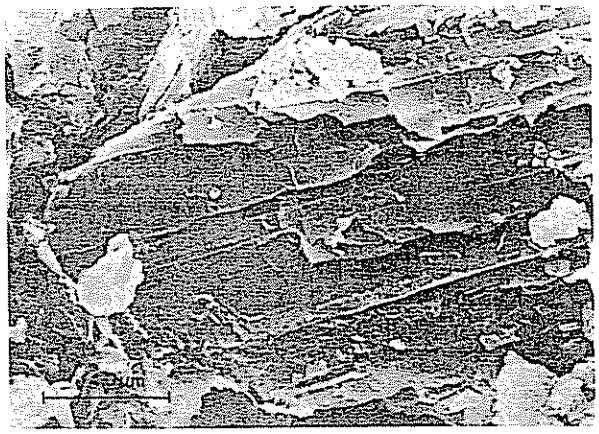

(a)

(b)

Fig. 9. (a) Filler particle cleavage in longitudinal orientation of grade 3499; (b) Across particle fracture in transverse orientation of grade 3499.

slightly tougher transverse orientation (Fig. 10). In contrast to the sharp differences in morphology of the transverse and longitudinal fracture surfaces for 3499, there is little apparent difference between the longitudinal (Fig. 11a) and transverse (Fig. 11b) fracture surfaces of KK-16. Fracture in this "isotropic" graphite is a combination of binder phase failure and the transgranular fracture of the fine-grained filler particles.

In direct contrast to the X-ray analysis, which indicates negligible preferred basal plane alignment, the lampblack-filled grade, 4029, exhibits strong slow crack growth anisotropy, the highest of any grade investigated (Fig. 12). Examination of the fracture surfaces reveals that the crack path lies exclusively in the binder phase for the longitudinal orientation (Fig. 13a). In contrast, numerous crack interactions with asymmetric "particles" are clearly observed in the tougher, transverse orientation (Fig. 13b). Interaction takes the form of particle fracture and extensive particle-binder interfacial failure, chipping of particle edges and occasional particle pullout from the binder matrix. A corollary SEM study of the preformed lampblack filler used in the fabrication of this graphite identified the asymmetric "particles" as aggregates composed of lampblack and binder (Fig. 13c) which are produced during the preforming processing step. The aggregates, which are composed of discrete polycrystalline lampblack particles in a binder matrix, appear as an isotropic entity in X-ray analysis (due to the absence of any crystallite alignment in the individual lampblack particles) despite some preferential alignment of the asymmetric particles in the artifact.

The asymmetric aggregates are preferentially oriented during the "uniaxial" molding process, in a manner similar to the individual crystallites shown in Fig. 2. This alignment leads to extensive crack-aggregate interaction for crack growth in the transverse orientation, while crack propagation in the longitudinal orientation occurs exclusively in the weaker binder phase.

From the extensive SEM fractography, some general micromechanical features appear to be common to all of the graphite materials observed here. Although the fracture path intersects pores of all sizes, it does not appear to preferentially seek out pores. Also, microcrack density increases, due to the crack tip stress field, appear to be minimal. Striations or microcracks visible in the petroleum coke filler particles are inherent structural features that probably result from thermal stresses during graphitization and subsequent cooling. In the longitudinal orientation of the petroleum coke artifacts, only those petroleum coke particles where the basal cleavage planes are nearly perpendicular to the applied stress are visible. This suggests that the crack is frequently deflected around mis-oriented coke particles and propagates through

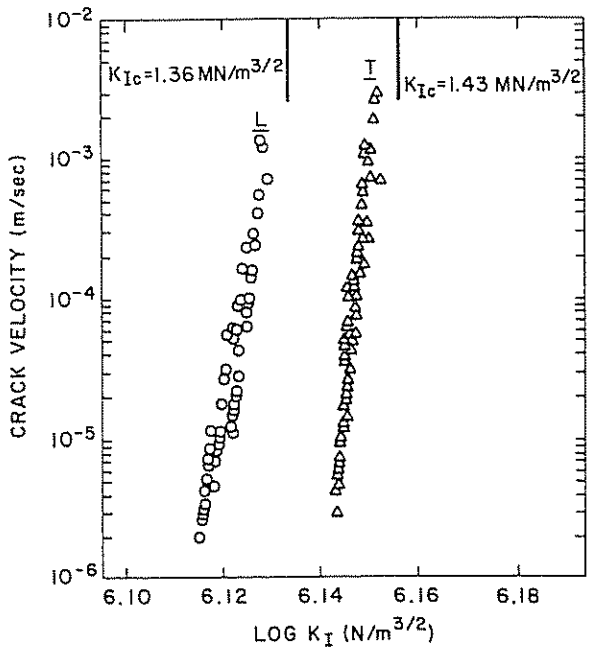

Fig. 10. Near-isotropic slow crack growth in grade KK-16.

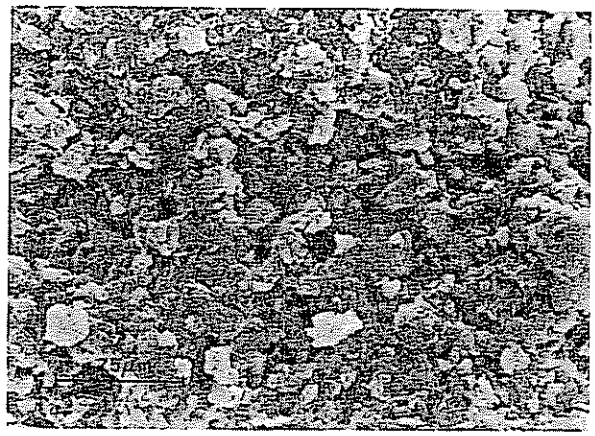

(a)

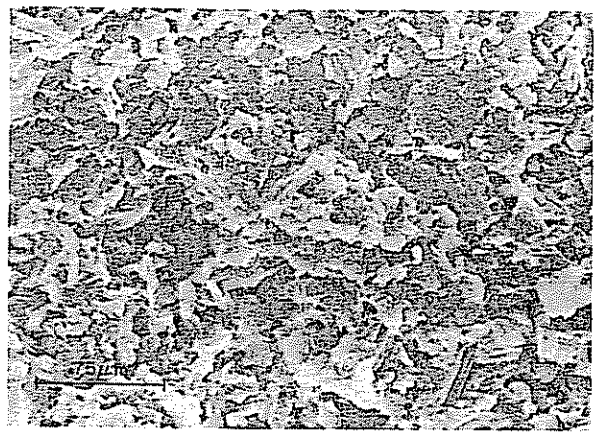

(b)

Fig. 11. (a) Longitudinal fracture surface of grade KK-16; (b) Transverse fracture surface of grade KK-16.

the binder phase. In the transverse orientation, however, particle fractures are quite numerous. Additionally, the tortuous crack path in the transverse orientation clearly substantiates that crack deflections around filler particles are quite common. Apparently, a combination of energy considerations and crystallite orientation determines whether a particle fractures or crack deflection around filler particles occurs in these materials.

Similar considerations apply to the lampblack-filled grade, 4029. Exclusive binder phase failure in the longitudinal orientation suggests that crack path deflections around the "preform" lampblack aggregates is energetically more favorable than aggregate fracture. In contrast, due to the asymmetry of the aggregates and their spatial distribution, the crack frequently fractures aggregates in the transverse orientation. It is important to note that, although the number of fractured aggregates is not large, this factor, coupled with a more tortuous crack path due to numerous deflections around aggregates, results in a substantial increase in toughness. For the lampblack material, therefore, processing and resultant aggregate orientation is of prime importance in determining fracture path and, consequently, the toughness. One might speculate that this material would exhibit isotropic behavior if processing of the preform completely excluded the aggregate particles.

The slow crack growth data for the graphites studied here are combined with available literature values for three other types of carbons in Fig. 14; (a) glassy carbons [20], (b) two phase artifacts, including a carbon refractory brick [21] and polycrystalline graphites (this study, 5), and (c) a pyrolytic graphite [22]. These three types of carbon can be characterized roughly as follows. Glassy carbons contain small, poorly-aligned crystallites with extensive cross-linking between them. These single phase carbons exhibit isotropic properties and the lowest toughnesses. Carbon artifacts are composites, consisting of two phases, a binder and a filler. The crystallite size and alignment in each of these two phases depends upon the processing and the precursors used to prepare the phases. For the artifacts considered in Fig. 14, there is a range of crystallite sizes, at least in the filler phase, but the size in each case far exceeds that of the glassy carbons. Antisotropy in toughness depends upon the extent of crystallite and/or filler particle alignment in these artifacts. Single phase pyrolytic graphite is characteristic of the other extreme, i.e. large, highly-aligned individual crystallites with negligible cross-linking between crystallites. This material exhibits properties which are highly anisotropic. When a crack is propagating across (or transverse) to the crystallite basal planes, pyrolytic graphite appears to be the toughest form of these three types of carbon.

In summary, single phase glassy carbons are the lowest toughness form of carbon. Single phase, highly crystalline pyrolytic graphite, fractured in a direction

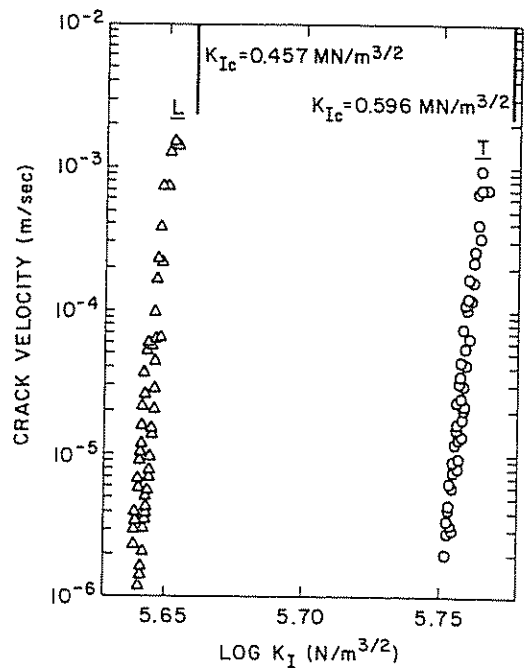

Fig. 12. Anisotropic slow crack growth in grade 4029.

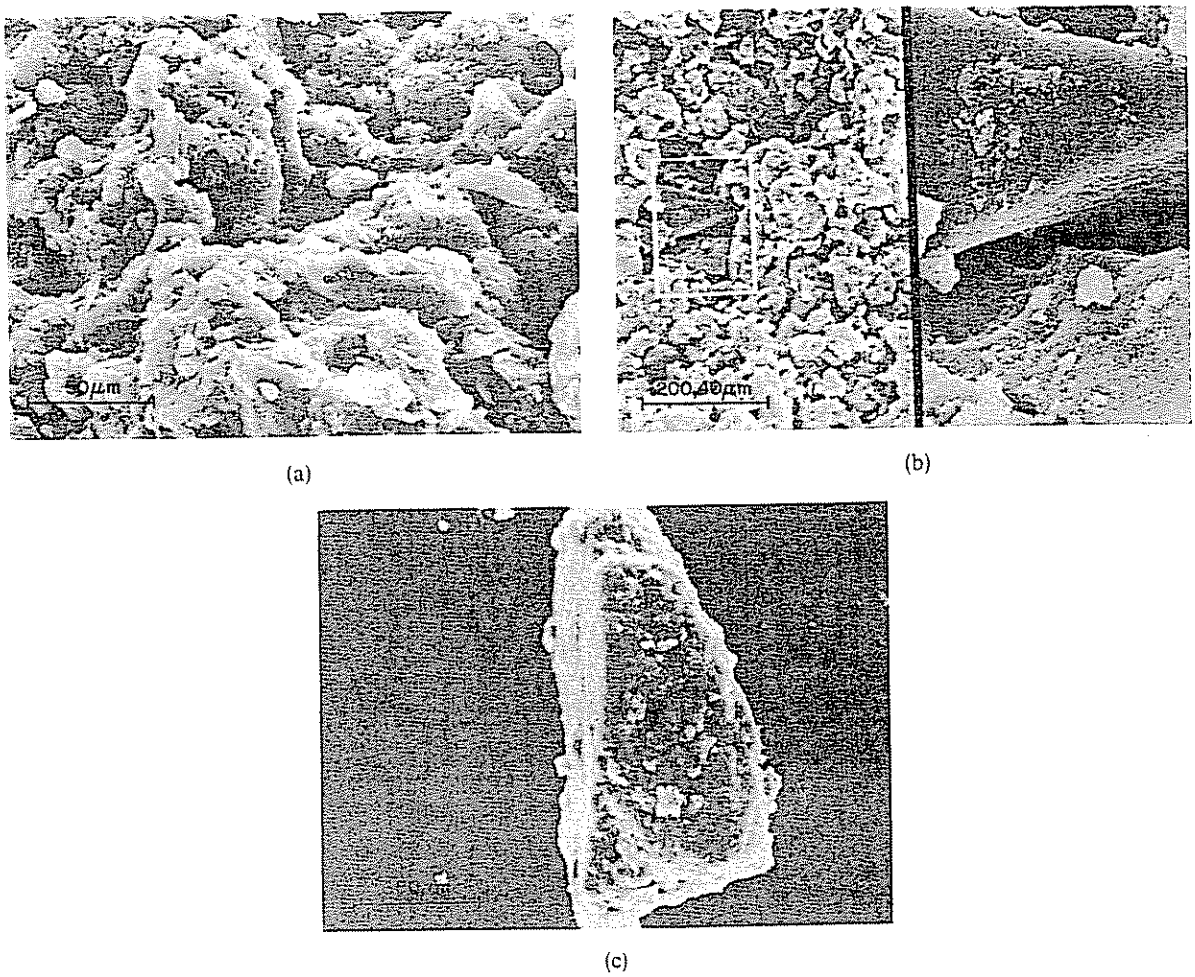

Fig. 13. (a) Longitudinal fracture surface of grade 4029, showing exclusive binder phase failure; (b) Transverse fracture surface of grade 4029, showing fracture of lampblack-binder aggregates; (c) As-received asymmetric lampblack-binder aggregate filler of grade 4029.

transverse to the crystallite basal planes, is the toughest form of carbon. "Composite" two phase graphites, a combination of the two extremes in varying degree, consist of a less-crystalline phase (binder) and a crystalline one (filler). The actual toughness and (K_I-V_I) behavior of these "composites" are dependent upon the relative fractions of the two phases, anisotropy in the artifacts, and porosity.

4. SUMMARY AND CONCLUSIONS

The room temperature subcritical crack growth of four commercial polycrystalline graphites was studied by the double-torsion method. A single region of slow crack growth behavior was observed in all materials at large fractions of their respective fracture toughness values, suggesting that crack growth is primarily governed by mechanical processes.

Preferred crystallite alignment in a petroleum coke-based graphite produced a tougher transverse orientation. In the longitudinal orientation, cleavage of suitably oriented filler particles and binder phase failure were observed. In the transverse orientation, transverse filler particle fractures and tortuous crack path deflections around filler particles were quite common.

Nearly isotropic slow crack growth behavior was observed in an isostatically molded petroleum coke-filled graphite. Fracture in this graphite occurred by a

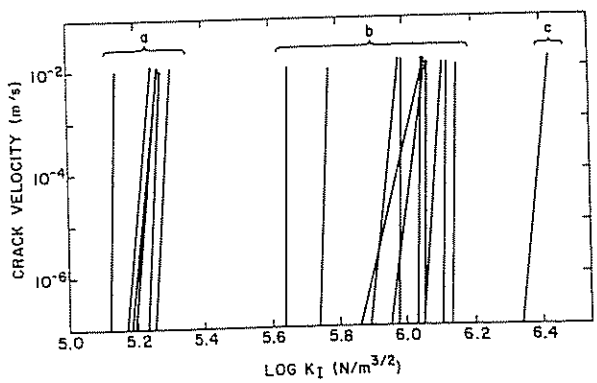

Fig. 14. Slow crack growth behavior of some carbons and graphites: (a) glassy carbons [20], (b) two-phase carbon and graphite artifacts (this study, 5, 21), and (c) pyrolytic graphite [22].

combination of binder phase failure and the transgranular fracture of the fine-grained filler particles.

Preferred alignment of asymmetric lampblack aggregates produced a tougher transverse orientation in a lampblack-filled graphite. Crack propagation in the longitudinal orientation of this graphite occurred exclusively in the binder phase. In contrast, fractured lampblack-binder aggregates and a more tortuous crack path were observed in the tougher transverse orientation.

Acknowledgements—This study was made possible by a grant from Airco Speer Carbon-Graphite. The assistance of Dr. Peter A. Thrower with the X-ray analysis and of Richard Pysz with the SEM fractography are also gratefully acknowledged.

REFERENCES

1. R. J. Diefendorf, *Proc. 4th Carbon Conf.*, pp. 489–496. Pergamon Press, New York (1960).
2. G. W. Rowe, *Nucl. Engr.* **7**, 102 (1962).
3. D. H. Logsdail, *AERE Report* 5721 (1968).
4. F. H. Vitovec and Z. H. Stachurski, *Carbon* **10**, 417 (1972).
5. S. W. Freiman and J. J. Mecholsky, *REVMAT Quart. Prog. Rep.* (Mar. 1975).
6. J. S. Nadeau and P. H. Hodkinson, *J. Mater. Sci.* **10**, 846 (1975).
7. G. M. Jenkins, *J. Nucl. Mater.* **5**, 280 (1962).
8. R. Taylor, R. G. Brown, K. E. Gilchrist, E. Hall, A. T. Hodds, B. T. Kelly and F. Morris, *Carbon* **5**, 495 (1967).
9. O. D. Slagle, *J. Am. Ceram. Soc.* **50**, 495 (1967).
10. T. Oku and M. Eto, *Carbon* **11**, 639 (1973).
11. J. E. Zimmer and R. A. Meyer, *12th Biennial Conf. on Carbon Abstracts*, p. 95. American Carbon Society (1975).
12. J. F. Andrew, J. Okada and D. C. Wobschall, *Proc. 4th Carbon Conf.*, pp. 559–575. Pergamon Press, New York (1960).
13. K. E. Gilchrist and D. Wells, *Carbon* **7**, 627 (1969).
14. G. Kraus and J. Semmler, *Carbon* **16**, 185 (1978).
15. S. Spinner and W. E. Tefft, *ASTM Proc.* **61**, (1961) 1221.
16. J. O. Outwater, M. C. Murphy, R. G. Kumble and J. T. Berry, *Fracture Toughness and Slow Stable Cracking*, pp. 127–138. ASTM STP 559. American Society for Testing and Materials (1974).
17. D. P. Williams and A. G. Evans, *J. Testing and Evaluation* **1**, 264 (1973).
18. J. L. Wood, Ph.D. Thesis. The Pennsylvania State University (1979).
19. S. M. Wiederhorn, *Fracture Mechanics of Ceramics* (Edited by R. C. Bradt, D. P. H. Hasselman and F. F. Lange), Vol. 2, pp. 613–646. Plenum Press, New York and London (1974).
20. W. P. Minnear, T. M. Hollenbeck, R. C. Bradt and P. L. Walker, Jr., *J. Non-cryst. Solids* **21**, 107 (1976).
21. J. L. Wood, Unpublished data.
22. J. S. Nadeau, *J. Am. Ceram. Soc.* **57**, 303 (1974).